Science of the Total Environment 562 (2016) 335–343

Contents lists available at ScienceDirect

Science of the Total Environment

journal homepage: www.elsevier.com/locate/scitotenv

Coprecipitation of ^{14}C and Sr with carbonate precipitates: The importance of reaction kinetics and recrystallization pathways

David J. Hodkin [a], Douglas I. Stewart [b], James T. Graham [c], Ian T. Burke [a,*]

[a] School of Earth and Environment, University of Leeds, Leeds LS2 9JT, UK
[b] School of Civil Engineering, University of Leeds, UK
[c] National Nuclear Laboratory, Sellafield, Cumbria, UK

HIGHLIGHTS

- 99.7% of ^{14}C and 98.6% of Sr removed from aqueous solution by $CaCO_3$ precipitation.
- Remobilization of ^{14}C observed during calcium carbonate recrystallization.
- Sr displayed variable distribution coefficient (possibly affected by Ca:Sr ratio).
- Reagent cost of \$0.22/m^3 of treated groundwater.

GRAPHICAL ABSTRACT

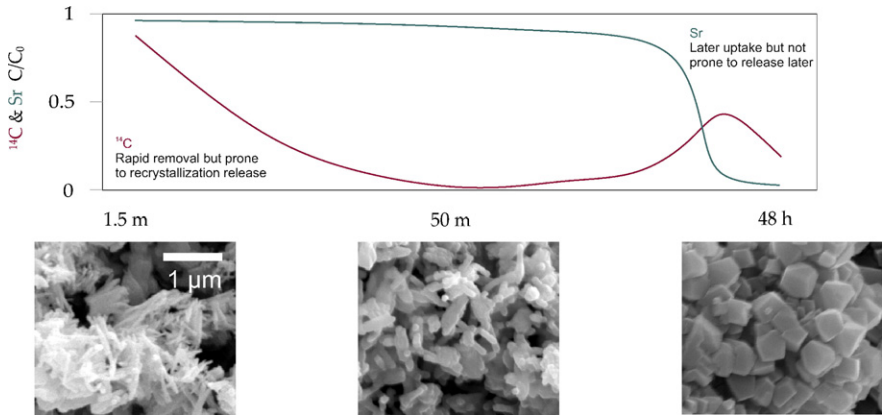

ARTICLE INFO

Article history:
Received 17 February 2016
Received in revised form 25 March 2016
Accepted 25 March 2016
Available online xxxx

Editor: Ajit Sarmah

Keywords:
Carbonate
Remediation
Nuclear
Radiocarbon
Strontium-90

ABSTRACT

This study investigated the simultaneous removal of Sr^{2+} and $^{14}CO_3^{2-}$ from pH > 12 $Ca(OH)_2$ solution by the precipitation of calcium carbonate. Initial Ca^{2+}:CO_3^{2-} ratios ranged from 10:1 to 10:100 (mM:mM). Maximum removal of ^{14}C and Sr^{2+} both occurred in the system containing 10 mM Ca^{2+} and 1 mM CO_3^{2-} (99.7% and 98.6% removal respectively). A kinetic model is provided that describes ^{14}C and Sr removal in terms of mineral dissolution and precipitation reactions. The removal of ^{14}C was achieved during the depletion of the initial TIC in solution, and was subsequently significantly affected by recrystallization of the calcite precipitate from an elongate to isotropic morphology. This liberated > 46% of the ^{14}C back to solution. Sr^{2+} removal occurred as Ca^{2+} became depleted in solution and was not significantly affected by the recrystallization process. The proposed reaction could form the basis for low cost remediation scheme for ^{90}Sr and ^{14}C in radioactively contaminated waters (<\$0.25 reagent cost per m^3 treated).

1. Introduction

The mining, milling and refining of nuclear fuels, accidents occurring during the operation of nuclear power facilities, and nuclear fuel

* Corresponding author.
E-mail address: I.T.Burke@leeds.ac.uk (I.T. Burke).

http://dx.doi.org/10.1016/j.scitotenv.2016.03.192
0048-9697/

reprocessing have left a legacy of groundwater pollution by radionuclides (Kersting et al., 1999; Naftz et al., 2002; Roehl et al., 2005). Radioactively contaminated ground and groundwater pose a potential threat to a number of receptors including drinking water resources, humans and non-human biota (Palmisano and Hazen, 2003; Stewart et al., 2006). Also the presence of even low levels of groundwater pollution will require continued oversight, and thus may negatively impact on the restoration of nuclear sites to beneficial use (NDA, 2013). ^{90}Sr is a high yield fission product that if ingested can substitute for Ca in bone (Nielsen, 2004). It is mobile in groundwater as the $^{90}Sr^{2+}$ ion and is a contaminant of concern at nuclear sites across the world (Gray et al., 1995; Saunders and Toran, 1995; Standring et al., 2002; Thompson et al., 2010). ^{14}C is a long lived neutron capture product that can be taken up by biota during assimilative respiration and growth (Amiro and Ewing, 1992). ^{14}C is an important component of all radioactive wastes and is potentially very mobile in groundwater as $H^{14}CO_3^-$. As a result ^{14}C is a contaminant of concern at many nuclear sites (Aquilonius and Hallberg, 2005; Dias et al., 2009; Magnusson et al., 2007; Roussel-Debet et al., 2006), and is known to have been released in large quantities at some sites (e.g. ^{14}C emissions averaged 8.13 TBq year^{-1} between 1994 and 2013 at the UK Sellafield nuclear site (Tierney et al., 2016).

At Sellafield, offsite measurements of groundwater ^{90}Sr and ^{14}C activities were below detection limits in 2013. However, in the same year within the site boundary, activities of up to 42 kBq L^{-1} of ^{90}Sr and 44 kBq L^{-1} of ^{14}C were reported (well above the WHO drinking water guidelines of 0.1 and 0.01 kBq L^{-1} respectively (Stamper et al., 2014)). While the WHO guidelines are not regulated concentration limits, treatment of these groundwaters may ultimately be necessary prior to eventual site closure. ^{90}Sr (as Sr^{2+}) and ^{14}C (as HCO_3^-) are in places co-located, therefore, a technique that can remove both ions in a single process would have advantages over other methods of groundwater treatment. Cation exchange media (e.g. zeolites and resins) are the primary technology currently used to remove ^{90}Sr from nuclear plant effluents, and to treat incoming plant make-up water (Marinin and Brown, 2000; "National Nuclear Laoratory, n.d"). Their operation relies on the displacement of weakly bound cations from a solid matrix by aqueous $^{90}Sr^{2+}$ ions. The approach can be very effective for the removal of high concentrations of ions from effluents; however, their applicability to low concentrations in groundwater is potentially problematic owing to the presence of competing ions (Barton et al., 2004). Contaminated groundwater tends to contain Sr^{2+} ions in concentrations of μg/L whereas other divalent metals such as Ca^{2+} and Mg^{2+} are present in mg/L concentrations. The competition from these groundwater ions for exchange sites can greatly reduce the effectiveness of any proposed treatment scheme based on ion exchange reactions. In addition, anionic contaminants such as ^{14}C in bicarbonate and carbonate ions (HCO^{3-} and CO_3^{2-}) would require a separate anion exchange process with similar competing ion issues from non-radioactive species.

Induced carbonate precipitation is an alternative approach that could potentially remove both ^{90}Sr and ^{14}C in a single process (Achal et al., 2012; Fujita et al., 2000; Mitchell and Ferris, 2005). Calcium hydroxide ($Ca(OH)_2$) is a relatively low cost reagent that is produced on a large scale for use in the construction and agricultural industries ("National Lime Association n.d"). Addition of calcium hydroxide to water containing HCO_3^- or CO_3^{2-} results in the rapid precipitation of calcium carbonate (Eqs. (1)–(4)) (Clark et al., 1992). Rapid precipitation of calcium carbonate can result in the co-precipitation of other metal ions (Curti, 1997).

$$Ca(OH)_{2(s)} \leftrightarrows Ca^{2-}{}_{(aq)} + 2OH^- \quad (1)$$

$$CO_{2(g)} \leftrightarrows CO_{2(aq)} \quad (2a)$$

$$CO_{2(aq)} + OH^- \leftrightarrows HCO_3^-{}_{(aq)} \quad (2b)$$

$$H_2CO_{3(aq)} \leftrightarrows HCO_3^-{}_{(aq)} + H^+ \leftrightarrows CO_3{}^{2-}{}_{(aq)} + H^+ \quad (2c)$$

$$Ca^{2+}{}_{(aq)} + CO_3{}^{2-}{}_{(aq)} \leftrightarrows CaCO_{3(s)} \quad (3)$$

Thus the net reaction is:

$$Ca(OH)_2 + CO_2 \leftrightarrows CaCO_3 + H_2O. \quad (4)$$

Coprecipitation of trace metals in carbonates occurs because of a similarity in the valence and ionic radius of the major carbonate M^{2+} ion (Ca^{2+}) and a range of minor ions (Sr^{2+}, Fe^{2+}, Cd^{2+}, Cu^{2+}). These minor ions may replace calcium within the carbonate lattice or adsorb to the growing mineral, causing their accumulation in the solid phase (Curti, 1997). Much of the early work on coprecipitation into carbonates focused on marine limestone and calcifying organisms (Holland et al., 1964; Katz et al., 1972; Pingitore et al., 1992). When treating ^{90}Sr and ^{14}C in contaminated groundwater sub-saturated with respect to carbonate, it is likely that the precipitate formed will undergo eventual dissolution. Therefore in these regimes it is likely that the groundwater will need to be extracted and treated ex-situ to give better process control, improve efficiency and facilitate the safe disposal of the radionuclide containing carbonates that are produced.

One of the factors which may affect the efficiency of ^{90}Sr and ^{14}C incorporation into carbonates will be the crystallization pathways the precipitate undergoes. Neo-formed precipitates are often unstable and their recrystallization can occur over time (Fernández-Díaz et al., 2010). Due to wide interest in the fundamentals of carbonate nucleation and growth, the crystallization pathways that occur during the precipitation of aqueous Ca^{2+} and CO_3^{2-} and eventual transformation to thermodynamically stable calcite have received a lot of research attention e.g.(Gebauer et al., 2008; Nielsen et al., 2014; Zhang and Dawe, 2000). Ostwald's rule of stages describes one of the common causes of morphological transitions during precipitation (Ostwald, 1897). The rule states that during nucleation the first formed phase is the most kinetically accessible, but this may not be the most thermodynamically stable. As precipitation progresses the kinetically accessible phase will transform to a thermodynamically stable one, potentially thorough a series of intermediaries. The consequences of recrystallization for trace metal co-precipitation have not yet been fully determined.

This paper reports an investigation of ^{14}C-carbonate and Sr uptake during calcium carbonate precipitation in both closed systems and systems that were open to atmospheric CO_2. We have characterized the crystallization pathways that were observed and the associate effects on ^{14}C and Sr uptake. A simple kinetic model is then proposed which identifies the controlling factors at different stages of the alkaline precipitation process, and indicates reaction stages that control the rate of ^{14}C and Sr uptake. Finally, the implications of the experimental results for a low cost treatment scheme for $^{14}C/^{90}Sr$ contaminated groundwater are discussed.

2. Experimental section

Calcium carbonate precipitation from alkaline solutions was investigated in triplicate batch experiments conducted in 500 mL polypropylene conical flasks (ThermoFisher Scientific, USA). The initial solution comprised of 100 mL of 0.01 M NaOH. This solution was used to provide an initial pH of 12 as it has been shown that at pH < 10 atmospheric exchange of ^{14}C is significant (Boylan et al., n.d.). Sr was added as $SrCl_2 \cdot 6H_2O$ to a concentration of 0.114 mM Sr^{2+} (10 ppm) and ^{14}C was added as $Na_2^{14}CO_3$ to an activity of 100 Bq mL^{-1}. These concentrations were used because they are easily measureable but remain close to the observed contamination levels at Sellafield (see S.I. S9). Natural groundwater Sr concentrations are low so the treatment strategy is to remove all aqueous Sr, thus it was unnecessary to use radiostrontium.

However the possibility of CO_3^{2-}/HCO_3^- exchange with atmospheric CO_2 meant it is important to understand the fate of aqueous ^{14}C. The solution was mixed by swirling on an orbital shaker. Calcium was then added as solid $Ca(OH)_2$ to a concentration equivalent to 10 mM, and simultaneously carbonate was added as Na_2CO_3 to concentrations of 1, 5, 10 and 100 mM. Thus the initial $Ca^{2+}:CO_3^{2-}$ ratios were 10:1, 10:5. 10:10 and 10:100 (mM:mM) (hereafter referred to as [Ca]10:[CO_3]1 etc…)

Air-permeable foam bungs were placed in the top of the conical flasks to prevent sample contamination, and the flasks were placed on an orbital shaker at 100 rpm for 200 h. Periodically the temperature and pH of the solutions in the flasks were measured and sub-samples were taken for chemical and mineralogical analysis. The sampling interval was increased from 30 s to 200 h as the experiment progressed to give data at approximately equal intervals of log(time).

Separate closed system experiments were carried out in 40 mL sealed reaction vessels with minimal headspace. These were run for 24 h and sampled at the same time intervals as the open system experiments.

3. Chemical analysis

Temperature and pH were measured using an Orion 420 pH meter with a VWR SJ113 probe calibrated at pH 4.01, 7.0 and 10.01. All aqueous samples were filtered using 0.2 μm Polyethersulfone hydrophilic filters. Sub-samples for metal analysis (0.5 mL) were added to 9.5 mL of 0.1 M Aristar® grade HNO_3 (VWR International, USA) for storage and analysed using inductively-coupled plasma, optical emission spectrometer (Thermo iCAP 7400, Thermo Fisher Scientific, Inc, USA). ^{14}C was measured by liquid scintillation counting (Tri-Carb 2100TR, PerkinElmer, USA); sub-samples of 0.5 mL were added to 9 mL of Hionic Fluor Liquid Scintillation Cocktail (PerkinElmer, USA) and 100 μL of 2 M NaOH and stored in the dark for 24 h before counting.

TIC (Total Inorganic Carbon) was analysed in a parallel series of experiments using the same starting conditions (excluding ^{14}C). Filtered aqueous samples were stored in 1.5 mL Eppendorf vials and frozen to prevent degassing of CO_2. TIC determinations were made by Flow Injection Analysis (FIA) following the method of Hall and Aller (Hall and Aller, 1992).

4. Mineralogical analysis

A series of sacrificial experiments were carried out to recover solids for X-ray diffraction (XRD) and scanning electron microscope (SEM) analysis from the [Ca]10:[CO_3]1 experiment. These employed the same starting conditions (excluding ^{14}C) as the precipitation experiments described above. Periodically an entire replicate was sacrificed and the solution was passed through a Buchner filter with Sartorius Stedim Polycarbonate Track-Etch Membrane filter paper. Solids were washed with isopropyl alcohol, and then stored in a desiccator.

The mineralogy of solids recovered by vacuum filtration was analysed using a Bruker D8 XRD with a Cu Kα source. Rietveld analysis (Rietveld, 1969) was carried out using Topas 4–2 to calculate relative proportions of carbonate polymorphs and $Ca(OH)_2$. The morphology of precipitates was observed using a FEI Quanta 650 FEG SEM. This also enabled observations to be made on changes in crystal size distribution and morphology, as well as looking for amorphous intermediaries.

5. Results

5.1. pH

The pH of all the precipitation experiments displayed a similar pattern with time regardless of the initial $Ca^{2+}:CO_3^{2-}$ molar ratio (Fig. 1). In all cases the pH was initially fairly stable at a value 12.2 ± 0.3 for approximately 24 h, and then decreased with time until the end of the tests. The rate of pH change was more rapid in experiments with lower initial CO_3^{2-} concentrations. The experimental series displayed a systematic increase in final pH, from 9.0 for [Ca]10:[CO_3]1 to 10.1 for [Ca]10:[CO_3]100. Temperature measurements indicated a temperature of 19.6 °C ± 0.8 during all experiments.

5.2. Calcium

The Ca concentration varied systematically with the initial $Ca^{2+}:CO_3^{2-}$ molar ratio. Experiments where Ca^{2+} was present in molar excess to the initial amount of CO_3^{2-} exhibited significant Ca^{2+} concentrations in solution (>10% C_o) for at least the first 8 h, before this dropped to <1% C_o. In contrast, the Ca^{2+} concentration in experiments where there were initially equal amounts of Ca^{2+} and CO_3^{2}, or an excess of CO_3^{2-}, dropped rapidly to <1% C_o over the first 5 min. In all experiments the Ca^{2+} concentration reached a minimum of 11.6 μM ± 1.1, before there was a slight increase contemporaneously with the decrease in pH. The final Ca^{2+} concentration was 21 μM ± 10 in all tests.

5.3. Strontium

The strontium concentration decreased from 114 μM to 0.02 μM ± 0.10 in all experiments. In all cases Sr removal from solution started after most of the Ca (>80%) had been removed from solution. The [Ca]10:[CO_3]5 experiment displayed a pause in Sr removal between 8 min and 6 h. Strontium showed a similar remobilization to calcium after 100 h increasing from 0.02 μM ± 0.10 to 0.40 μM ± 0.20 by 200 h.

5.4. TIC

All experiments displayed an initial decrease in TIC concentration lasting until 8 min in high $Ca^{2+}:CO_3^{2-}$ molar ratios and 50 min in experiments with low $Ca^{2+}:CO_3^{2-}$ molar ratios. In experiments with high $Ca^{2+}:CO_3^{2}$ molar ratios the initial decrease in TIC was followed by an interval of uniformly low TIC after which TIC began to accumulate. Experiments with low $Ca^{2+}:CO_3^{2-}$ molar ratios did not display this interval of uniform TIC concentration, but instead showed immediate TIC accumulation following the initial depletion.

5.5. Carbon-14

Carbon-14 removal varied systematically with the experimental conditions. Maximum removal (99.7%) was observed at 50 min during the [Ca]10:[CO_3]1 experiment. However this experiment also displayed a significant remobilization starting after 50 min, which reached a maximum after 72 h. Experiments with higher $Ca^{2+}:CO_3^{2-}$ molar ratios displayed progressively less ^{14}C removal but with lower remobilization.

5.6. Morphology

The XRD analysis of precipitate recovered from the [Ca]10:[CO_3^{2-}]1 sacrificial experiments showed that the initial precipitate (t = 1.5 min) was calcite, and that this was the only new crystalline phase identified during the experiments (Supporting information Section 1). SEM analysis indicates an elongate morphology characterized by an average length of 490 nm and width of 110 nm was present after 1.5 min, which displayed growth along the elongate axis to 590 nm by 110 nm by 50 min (Fig. 2). After 50 min the morphology of the precipitate changed, becoming more isotropic (460 nm by 410 nm). This transition was complete by 190 h.

5.7. Closed system

Closed system (Supporting information Section 2) displayed a stable pH > 12 throughout the experiments. Initial calcium trends were similar to those observed in the equivalent open system experiments. In experiments where there were initially equal amounts of Ca^{2+} and CO_3^{2}, or an

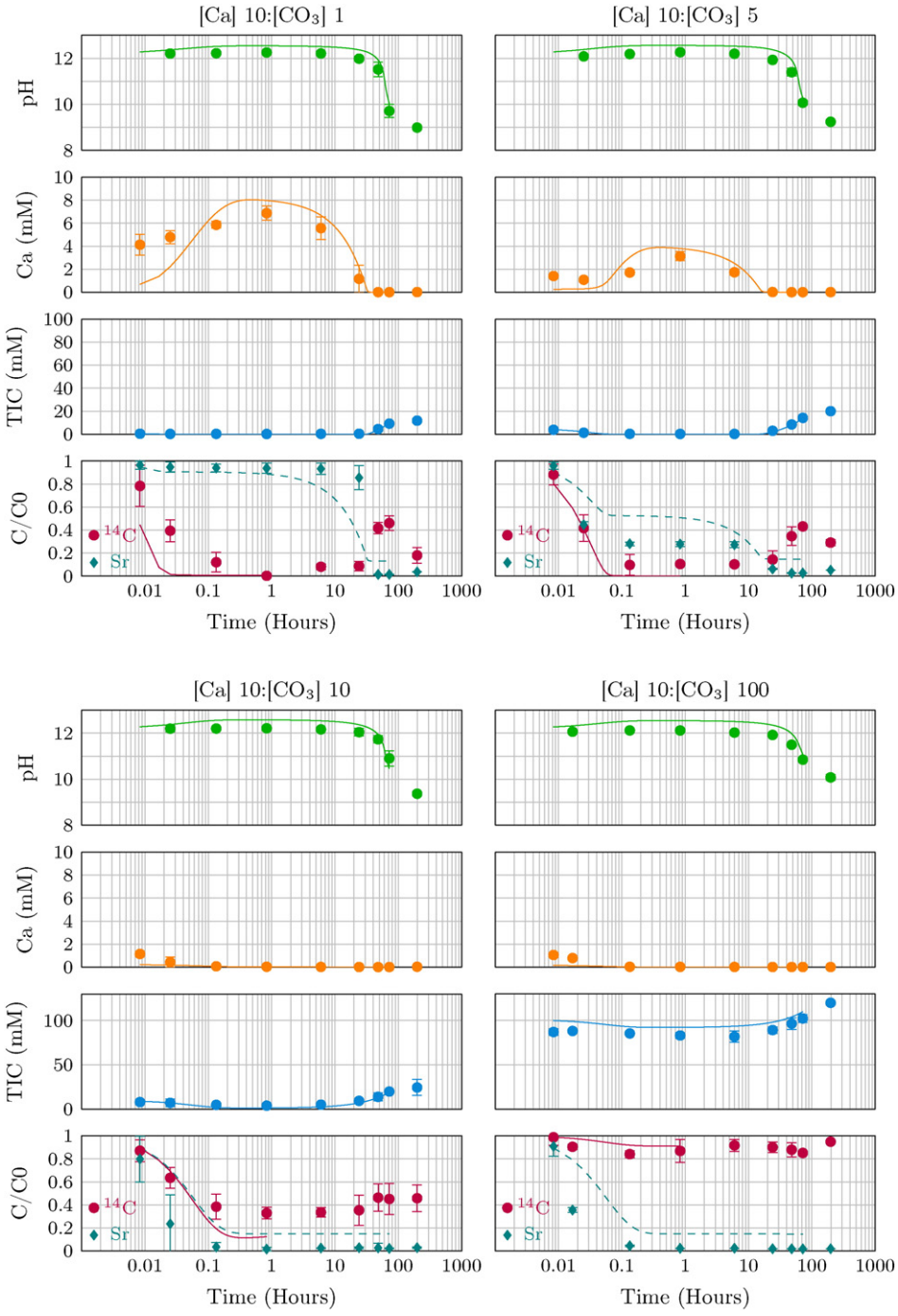

Fig. 1. Solution composition for the open system experiments alongside model data computed in PHREEQC. The model for ^{14}C removal was run until max TIC depletion which occurred at 50 min, after which in-gassing became important. All other data was modelled for 72 h. (Data tables are included in SI S3).

excess of CO_3^{2-}, the Ca^{2+} concentrations reduced rapidly to <1% of initial concentrations (C_o) over the first 5 min; but where Ca^{2+} was present in molar excess, a significant aqueous Ca^{2+} concentrations developed over the first hour. However, in the closed [Ca]10:[CO_3^{2-}]1 system there was no subsequent drop in aqueous Ca^{2+} concentration at longer time periods. Near complete strontium removal occurred in the systems where [CO_3^{2-}] ≥ [Ca^{2+}], but very little strontium removal was observed where Ca^{2+} was present in molar excess to CO_3^{2-}. A small amount of strontium was remobilized after 24 h in the experiment where initial Ca^{2+} and CO_3^{2-} concentrations were close to stoichiometric balance. The removal of ^{14}C was less effective in the closed system experiments than in the equivalent open systems (e.g. a maximum of ~90% removal was observed in the closed [Ca]10:[CO_3^{2-}]1 system versus 99.7% removal in the open systems), but there was no significant remobilization of ^{14}C over time.

6. Interpretation

The pH of all the precipitation experiments was initially controlled by NaOH (pH > 12) and the subsequent rapid dissolution of $Ca(OH)_2$. Where there was in-gassing of atmospheric CO_2, the pH was buffered downwards by hydroxylation (Eq. (2b)), and the system transitioned to a carbonate buffered (pH ~9) system after 24 h. Closed system experiments did not show this pH drop due to the lack of atmospheric CO_2 in-gassing.

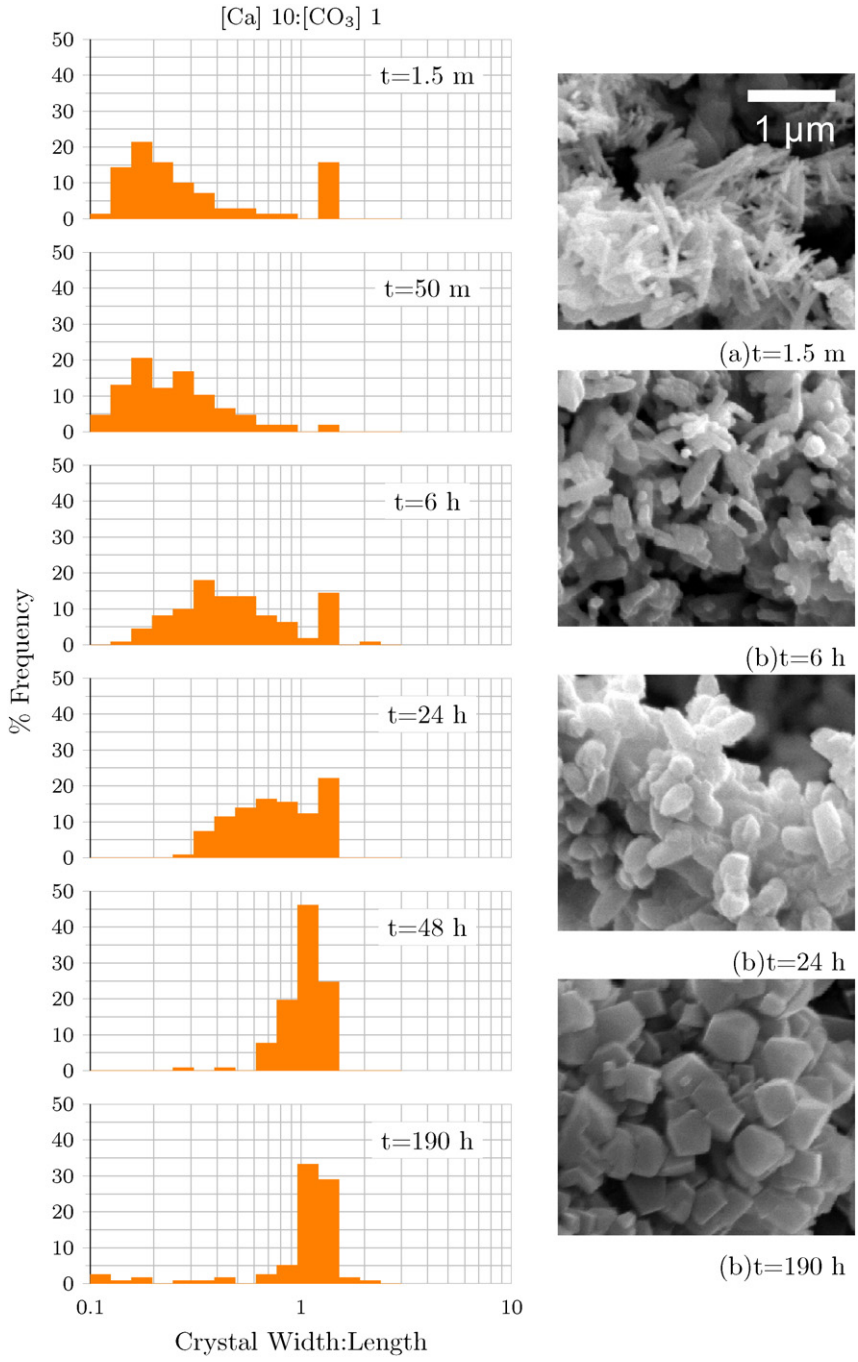

Fig. 2. Histograms displaying crystal width:length ratios of >100 crystals at 6 time points throughout the [Ca]10:[CO_3]1 experiment, with key SEM images for illustration.

Calcium hydroxide was added as a solid and will have dissolved until it became saturated. The [Ca]10:[CO_3^{2-}]1 and [Ca]10:[CO_3^{2-}]5 experiments displayed an increase in the concentration of Ca^{2+} corresponding to this dissolution between 30 s and 50 min. The rate of increase will have been a function of both $Ca(OH)_2$ dissolution and calcium carbonate precipitation. Once the solid $Ca(OH)_2$ was exhausted, all the open experiments displayed a trend of decreasing aqueous Ca^{2+} concentration with time. This was due to the precipitation of calcium carbonate, which is supported by both the SEM images and the XRD analysis of the [Ca]10:[CO_3^{2-}]1 system. Where there was stoichiometric excess of CO_3^{2-} in the initial solution the removal of Ca^{2+} was rapid, because Ca^{2+} from the dissolving $Ca(OH)_2$ was able to react immediately with CO_3^{2-} in the initial solution. These systems displayed a rate of calcium carbonate precipitation that was controlled by the rate of $Ca(OH)_2$ dissolution. In the [Ca]10:[CO_3^{2-}]1 and [Ca]10:[CO_3^{2-}]5 experiments, where there was stoichiometric excess of Ca^{2+}, the aqueous Ca^{2+} concentration initially increased, and only decreased once the solid $Ca(OH)_2$ was exhausted and in-gassing of atmospheric CO_2 into the alkaline solution resulted in calcium carbonate formation. In these systems the rate of calcium carbonate formation was controlled by the rate of CO_2 in-gassing once the CO_3^{2-} in the initial solution was exhausted.

The control of CO_2 in-gassing for the calcite precipitation rate is supported by the TIC trend, which displays depletion to minimum values within 8 min in experiments with initial stoichiometric excess of Ca^{2+}. This depletion was followed by an interval where TIC was maintained at low concentrations, indicating any TIC in-gassing was being rapidly used by carbonate precipitation. Experiments with initial

stoichiometric excess of CO_3^{2-} also show an initial depletion of TIC. However, this depletion was immediately followed by an increase in TIC (observed at the end of all experiments) caused by in-gassing of CO_2 in the absence of carbonate precipitation.

The initial morphology of solids recovered from the sacrificial [Ca]10:[CO_3]1 experiments was similar to that observed by Jung et al. (2000) under excess Ca conditions. It was suggested that the elongate shaped calcite results from excess Ca adsorption at the growth surface of the rhombohedral {104} faces which slows their growth. After 50 min a transition from elongate to isotropic calcite occurred which continued until the end of the experiment at 198 h. The cause of this transition is unclear as it initiated around the peak aqueous Ca^{2+} concentration when aqueous CO_3^{2-} was negligible (an interval during which the elongate form should be strongly favoured).

7. Modelling

Kinetic modelling was carried out using PHREEQC version 3 (Parkhurst and Appelo, 2013) and the Hatches database (Cross and Ewart, 1991) to better explain the key trends observed in the data (the full input text is available in Supporting information Section 4). Review of the data suggests the variation in the bulk chemistry of the reaction with time depends on the kinetics of at least three processes: the rate of $Ca(OH)_2$ dissolution, the rate of calcite precipitation, and the rate of CO_2 in-gassing.

Calcium hydroxide dissolution was modelled using the rate equation (Eq. (5)) proposed by Johannsen and Rademacher (1999).

$$R_{Port} = k_b \cdot S_p \cdot \left(K_{sp} - \alpha\left\{Ca^{2+}\right\} \cdot \alpha\{OH^-\}^2\right) \quad (5)$$

Where S_p is the surface area of $Ca(OH)_{2(S)}$ and $\alpha\{X\}$ is the aqueous activity of X (calculated in PHREEQC from aqueous concentration using the Debye-Hückel formula (Parkhurst and Appelo, 1999)). Implicitly equation (Eq. (5)) assumes that the rate limiting step controlling the rate of the reverse reaction is a tri-molecular elementary reaction. The forward and reverse constants suggested by Johannsen and Rademacher are $k_f = 1 \times 10^{-5}$ mol L^{-1} s^{-1} m^{-1} and $k_b = 2.1$ L^2 mol^{-2} s^{-1} m^{-2} at 20 °C (Johannsen and Rademacher, 1999). The ratio of the forward and reverse rate constants imply a solubility product for calcium hydroxide dissolution of 4.8×10^{-6}. This value is fractionally lower than the commonly used value of $K_{sp} = 5.5 \times 10^{-6}$, (Lide, 2001) but the difference is probably associated with the sensitivity of the reverse reaction to the amount of solid present (Johannsen and Rademacher, 1999). A specific surface area of 4.18 m^2 g^{-1} was derived from BET measurements of the $Ca(OH)_2$ starting material (Supporting information Section 5). In order to account for decreasing particle size during the dissolution the initial surface area was multiplied by the ratio of current moles to initial moles of $Ca(OH)_{2(s)}$. The initial amount of $Ca(OH)_2$ added to the system was assumed to be 9.2 mmol (rather than 10 mmol) to account for the 8% ± 3% calcite impurities observed in the $Ca(OH)_2$ stock, identified by XRD and quantified by Rietveld analysis.

Estimating the surface area of $Ca(OH)_{2(S)}$ from its mass would slightly underestimate the rate of dissolution if the $Ca(OH)_{2(S)}$ consisted of uniform equidimensional particles, as volume would decrease with the nominal particle size more quickly than would the surface area. However if the $Ca(OH)_{2(s)}$ assemblage contained a range of particle sizes, then the complete dissolution of fine crystals on short time scales would result in a decrease in the overall dissolution rate over longer time periods. Separate $Ca(OH)_2$ dissolution experiments were conducted to investigate the rate of $Ca(OH)_{2(S)}$ dissolution under the conditions used in this study (Supporting information Figure S3). These show that the rate equation assumed in the model underestimates the rate of dissolution over the first 2 min, and then overestimates the rate slightly; however, the Johannsen and Rademacher rate equation provides a good approximation to the observed data.

The Nancollas and Reddy model (Nancollas and Reddy, 1971) was used to predict calcium carbonate precipitation rates. This model was selected as it is based on the direct reaction of Ca^{2+} ions with CO_3^{2-} ions to form $CaCO_3$ (Eq. (6)), which is believed to be the main reaction pathway at pH > 9 (Inskeep and Bloom, 1985).

$$R_{Cal} = k_f \cdot S_c \cdot \left(\alpha\left\{Ca^{2+}\right\} \cdot \alpha\left\{CO_3{}^{2-}\right\} - K_{sp}\right). \quad (6)$$

Where k_f is the second order rate constant for calcite precipitation ($k_f = 118$ dm mol^{-1} m^{-2} s^{-1} (Inskeep and Bloom, 1985)), K_{sp} is the solubility product constant for calcite ($K_{sp} = 10^{-8.44}$ (Lide, 2001)), and S_c is the calcite surface area available for reaction. The surface area of neo-formed calcite could not be derived from BET analysis due to low precipitate yields as well as the presence of $Ca(OH)_2$ alongside the early formed precipitate. Surface areas were instead calculated from the average crystal dimensions from SEM images (Fig. 2) using an assumed calcite density of 2.7 g cm^{-3} and assuming a cubic shape for rhombic crystals and a cylindrical shape for prismatic crystals. Due to the presence of small masses of high surface area cylindrical crystals early in the experiment, which transformed and grew to higher masses of lower surface area rhombic crystals by the end of the experiment, the surface area likely remained relatively constant. However due to uncertainties in the mass of $CaCO_3$ precipitated at early time points a value of 5.4 m^2 g^{-1} was used, which reflects the maximum surface area associated with the rhombic endpoint (based on the conversion of 10 mM of $Ca(OH)_2$ to $CaCO_3$). The estimated calcite surface area value used is consistent with those observed in the literature (Supporting information Section 6).

The chemical equation for the uptake of $CO_{2(aq)}$ into an aqueous solution are shown in Eq. (2) (Clark et al., 1992). Deprotonation reactions such as (Eq. (2c)) are rapid in aqueous solution, therefore, in systems not limited by mixing, the rate at which atmospheric CO_2 enters solution will be controlled either by dissolution (Eq. (2a)) or hydroxylation (Eq. (2b)).

Noyes et al. (1996) suggest that the dissolution of CO_2 into an aqueous solution can be explained by contact between a gas phase and a homogenous solution when the reaction vessel was stirred vigorously enough to prevent a saturated surface layer forming. They report that gas dissolution flux of CO_2 per unit interface area (mol cm^{-2} s^{-1}) was:

$$J_{CO2} = k_{tr} \cdot \left(\left[CO_{2(aq)}\right]^{equilibrium} - \left[CO_{2(aq)}\right]\right). \quad (7)$$

Where k_{tr} is the exchange coefficient ($k_{tr} = 5.4 \times 10^{-4}$ cm s^{-1}), $[CO_{2(aq)}]$ is the aqueous concentration of CO_2 and $[CO_{2(aq)}]^{equilibrium}$ is the aqueous CO_2 concentration at equilibrium, calculated by Henry's law (Eq. (8)) (Atkins and De Paula, 2006):

$$\left[CO_{2(aq)}\right]^{equilibrium} = K_H \cdot P_{CO2}. \quad (8)$$

Where P_{CO2} is the partial pressure of CO_2 in the atmosphere ($P_{CO2} = 4 \times 10^{-4}$) and K_H is the Henry's law constant ($K_H = 0.034$ mol L^{-1} atm^{-1} for the dissolution of CO_2 in water (Sander, 2015)). Thus $[CO_{2(aq)}]^{equilibrium}$ is 1.36×10^{-5} mol L^{-1}. The maximum rate of CO_2 dissolution will occur when $[CO_{2(aq)}] = 0$ and is equal to 7.34×10^{-9} mol cm^{-2} s^{-1}. If the solution surface area in a 100 mL flask is 56 cm^2 (10.5 cm diameter) the CO_2 dissolution rate will be 1.48 mmol hr^{-1}.

The subsequent hydroxylation of this $CO_{2(aq)}$ by hydroxyl ions will have a forward reaction rate of the form:

$$R_{hyd} = k_{hyd} \cdot [CO_2(aq)] \cdot [OH^-]. \quad (9)$$

Where the rate constant $k_{hyd} = 5900$ L mol^{-1} s^{-1} (Pinsent et al., 1956). The theoretical maximum hydroxylation rate occurs when there is an equilibrium between atmospheric and dissolved CO_2. At pH 12.3 ($[OH^-]$ ~ 0.02 mol L^{-1}), which equates to a rate of 5777 mmol L^{-1} h^{-1}. Thus in a 100 mL solution at pH 12.3 the theoretical maximum hydroxylation rate of CO_2 is 578 mmol hr^{-1}. This suggests that in a highly alkaline system, that is initially very under-saturated with respect to carbonate species, the CO_2 dissolution rate will control the carbonate flux.

Fig. 3a shows the variation in Ca^{2+}(aq) in the [Ca]10:[CO_3]1 test for the time period between 50 min and 24 h. This system has a stoichiometric excess of Ca^{2+} and during this time period (after the calcium hydroxide had dissolved but while the pH > 12) it is believed that the aqueous calcium concentration is controlled by the CO_2 flux to solution. If this assumption is correct, the experimental observed flux of CO_2 into solution is constant during this time period, and equivalent to 0.25 mmol hr^{-1} into 100 mL of solution.

Fig. 3b shows the increase in TIC in the [Ca]10:[CO_3]10 test for the time period between 50 min and 72 h. This system was initially in stoichiometric balance, but the data are for the time period once Ca^{2+} had been removed from solution, and while the pH > 12. During this period it is believed that the dissolved TIC concentration is controlled by the CO_2 flux to solution. If this assumption is correct, the experimental observed flux of CO_2 into solution is constant during this time period, and is equivalent to 0.22 mmol hr^{-1} into 100 mL of solution. This is very similar to the CO_2 flux observed in the [Ca]10:[CO_3]1 test, and both about one sixth of the theoretical maximum dissolution flux of 1.48 mmol hr^{-1} calculated from (Eq. (8)).

The maximum $CO_{2(g)}$ dissolution rate predicted by (Eq. (8)) is equivalent to consuming the total amount of CO_2 in the headspace of a 500 mL conical flask (~500 mL) in ~40 s. The neck of the conical flasks was "stoppered" with foam bungs designed to stop contamination with atmospheric dust, but allow gas exchange with atmosphere by diffusion. It is probable that diffusion through the foam bung was unable to match the maximum rate of CO_2 dissolution, and the partial pressure CO_2 within the head-space of the flask was below its atmospheric value. An atmospheric P_{CO2} of 6.75×10^{-5} (1/6th atmospheric) yields a forward rate consistent with the experimental data.

The experimental rate begins to deviate from 0.25 mmol hr^{-1} as TIC accumulates in solution. As TIC accumulates the [$CO_{2(aq)}$] will increase and the reverse term in equation (Eq. (7)) becomes important. Without this reverse term the in-gassing would proceed unrestricted and predict a lower than observed final pH (Supporting information Section 7). PHREEQC distributes $CO_{2(aq)}$ into the H_2CO_3 "pool" therefore the [H_2CO_3] was used in the model in place of [$CO_{2(aq)}$]. This reverse rate will therefore be an overestimation of the out-gassing. However due to the low concentrations of H_2CO_3 and $CO_{2(aq)}$ at high pH this effect will be minimal. Supporting information Figure S4 shows that the models including and excluding the reverse term are able to bracket the observed data.

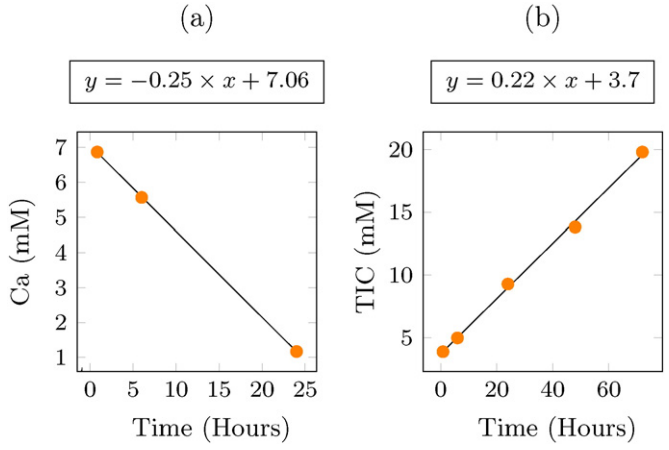

Fig. 3. a) Excerpt from the [Ca]10:[CO_3]1 Ca plot between 50 min and 24 h. b) Excerpt from the [Ca]10:[CO_3]10 TIC plot between 50 min and 72 h.

Carbon-14 removal was modelled assuming its removal would be proportional to that of initial TIC, and that isotopic affects are minimal. The ^{14}C C/C_o modelling shown in Fig. 1 is terminated at the point of maximum ^{14}C removal (after the initial TIC is depleted) as CO_2 in-gassing affects this trend. This was the case for all systems apart from the [Ca]10:[CO_3^{2-}]1 experiment which showed significantly more rapid ^{14}C depletion than TIC. This could be due to errors in the TIC measurements (near to the limit of detection), which become less significant at higher concentrations.

Sr removal was modelled assuming that (Sr,Ca)CO_3 is an ideal solid solution with a distribution coefficient of 0.057. This value was chosen as an average of experimental values (Supporting information Section 8) and concurs with literature values (Curti, 1997).

8. Discussion

Carbon-14 uptake was controlled by the depletion of TIC from solution. This was achieved most effectively where there was a stoichiometric excess of Ca^{2+} in solution. However, a recrystallization process which started after about 50 min caused a remobilization of ^{14}C to the solution. This remobilization indicates that the recrystallization involved a significant amount of dissolution which returned the lattice material to the solution, where the ^{14}C was diluted by $^{12}CO_2$ derived from in-gassing. Between 50 min and 24 h the remobilization observed in the [Ca]10:[CO_3^{2-}]1 experiment was limited and ^{14}C removal remained >89%. In this case the remobilization was limited because the $^{14}CO_3^{2-}$ was released into a solution with high Ca and low TIC and was therefore *re*-precipitated. After 24 h TIC began to accumulate in solution and so $^{14}CO_3^{2-}$ released by recrystallization also accumulated in solution. This suggests that if a net negative flux of TIC was maintained during the recrystallization ^{14}C would not accumulate in the solution.

In the closed system experiments the lack of CO_2 in-gassing ensured minimal TIC in solution to dilute any ^{14}C remobilized. However, this lack of CO_2 appears to have resulted in a lower ^{14}C removal across all experiments, likely due to the lower overall volume of calcite precipitated.

Sr removal was in excess of 97% under all experimental conditions (the maximum observed removal was 98.6% in the [Ca]10:[CO_3^{2-}]1 experiment). Sr removal occurred within the first 8 min in experiments with a stoichiometric excess of TIC, this Sr removal was associated with a depletion of Ca. Experiments with stoichiometric excess of Ca displayed a lag before the removal of Sr. Between 6 and 24 h 4.4 mmol of Ca (47%) was precipitated, accompanied by 0.78 ppm of Sr (7.8%). During the following interval (24–48 h) 1.2 mmol of Ca was precipitated (13%), accompanied by 8.4 ppm of Sr (84%). This suggests that an incorporation mechanism was operating between 24 and 48 h that was not occurring during the preceding interval.

A possible mechanism that explains the observed changes in Sr uptake involves the mode of Sr adsorption to the calcite surface. As Sr^{2+} concentration increases relative to Ca^{2+}, Sr incorporation may proceed via a strontianite like precursor rather than simple substitution for Ca in calcite (Parkman et al., 1998), producing a higher overall Sr uptake to solids (as observed in the later stages of our experiments). Further work would be required to prove this mechanism, however the results are consistent with a more effective incorporation route following the depletion of solution Ca; potentially indicating that the concentration of Sr relative to Ca may play a role in the effective removal of Sr. The [Ca]10:[CO_3^{2-}]5 experiment showed composite behaviour of the two series. Initially Sr was removed rapidly due to low concentration of Ca in solution simultaneous with dissolution of $Ca(OH)_2$ and precipitation of $CaCO_3$. Following this initial depletion there was a period during which Sr concentration remained stable ($\pm$0.1 ppm). This is

due to the accumulation of Ca in solution following the dissolution of $Ca(OH)_2$ into a TIC depleted solution.

A similar strontium removal from solution was achieved in all systems. It is possible that Sr was also remobilized during calcite recrystallization in the [Ca]10:[CO_3^{2-}]1 experiment, however, in contrast to the situation with ^{14}C, there is no additional source of M^{2+} cations in the solution, and as such, Sr was immediately re-precipitated and did not accumulate in solution.

The Sr and Ca concentration at the final time-points in all experiments were higher than the concentrations at the penultimate time points. This is a function of decreasing solution pH, which will have caused the dissolution of calcite. In the experiments where there was an initial stoichiometric excess of Ca^{2+} there is a loss of ^{14}C from solution in the final stages of experiments. These experiments reached a final pH < 9.3, and so this loss is attributed to isotopic exchange of aqueous ^{14}C with atmospheric $12CO_2$, which has be found to be a significant process in solutions with pH ≤ 9.3 (Boylan et al., n.d.).

9. Implications for groundwater treatment

A representative composition for groundwater in the Sellafield Separation Area is reported in (Supporting information Section 9) (Graham, 2013). Dosing such groundwater with calcium hydroxide to produce a solution with a pH > 12 and a stoichiometric excess of Ca^{2+} over CO_3^{2-} (i.e. conditions similar to those in the [Ca]10:[CO_3^{2-}]1 experiment) is a promising method for removing ^{14}C and ^{90}Sr. This would be most effective if it were operated as a two stage treatment scheme. The first stage would comprise of adding $Ca(OH)_2$ in a closed system to remove TIC, and thus the ^{14}C, from solution. After separation of the precipitate, the aqueous effluent would then be sparged with air to promote CO_2 in-gassing and induce further carbonate precipitation, which would co-precipitate the ^{90}Sr and decrease the pH. Based on the amounts of chemicals required to achieve the desired ratio of [Ca]10:[CO_3^{2-}]1 this treatment would have a reagent cost of approximately $0.22/m^3 (Supporting information Section 10).

Mass balance calculations were carried out using the maximum removal efficiencies of 99.7% for ^{14}C and 98.6% for Sr observed in our experiments (from the Ca 10 mM: 1 mM CO_3^{2-} experiment). These removal efficiencies were extrapolated to a treatment scheme involving 12.3 mM Ca and 1.23 mM CO_3^{-2} based on the most contaminated groundwater at Sellafield (14C = 50 kBq L^{-1}; Sr = 44 kBq L^{-1}; ~0.01 mM total Sr). The radioactive contaminants are distributed within the total DIC and Sr. The DIC and Sr concentrations are similar, or in the case of Sr, lower than experimental concentrations. Therefore, the Sr removal efficiency used may be conservative. The potential effects of other Sellafield groundwater ions, such as Mg^{2+} and SO_4^{2-}, that are known to affect calcite crystallization pathways at high concentrations (Bots et al., 2011), is expected to be minimal due to the low concentration of these ions (~0.2 mM) in the groundwater. These calculations suggest that 1 m^3 of the most contaminated groundwater present at Sellafield would precipitate 287 g of calcite during the ^{14}C removal phase, which would contain 49.85 MBq of ^{14}C. The ^{90}Sr removal phase would yield a further 943 g of calcite which would contain 43.38 MBq of ^{90}Sr. This would constitute a material with a total β activity of 75 GBq/ton (>6× the upper limit for Low Level Waste (Laker et al., 2010)); however, treatment of lower activity groundwater would in practice produce materials with much lower activities.

This process would also produce discharge water containing 0.15 KBq L^{-1} of ^{14}C and 0.62 KBq L^{-1} of ^{90}Sr. This effluent could be further treated by Ion Exchange media (having reduced the competing ions Ca and Mg during the calcite precipitation process) or simply discharged, depending on acceptable discharge limits. The proposed treatment would also produce an effluent stream buffered to pH < 9 (which is typically a desired pH limit for effluent discharges to surface waters (Mayes et al., 2009)). Finally, it is noted that the proposed two-stage treatment scheme would create separate waste products for ^{14}C and ^{90}Sr and does not result in an increase in liquid volume. Therefore, this treatment shows significant potential as a working remediation technique but further work is still required to understand how the proposed treatment scheme would function in site specific groundwater regimes. For example it is not known how the presence of Mg^{2+} and SO_4^{2-} in groundwater would affect the treatment (as these groundwater ions can affect the morphology and allotropes of carbonate precipitates (Bots et al., 2011)), or how the treatment efficiencies would scale to a smaller Sr^{2+} concentrations (i.e. 1.4 μM vs 114 μM). The overall cost effectiveness of this treatment will also be affected by in-situ rates of contaminant desorption/dissolution from solids, which may result in the need for continued groundwater removal and treatment over long time periods.

10. Conclusion

The precipitation of calcium carbonate has been shown to be a viable mechanism for the removal of ^{14}C and Sr from a solution. Overall, the maximum achieved removal of ^{14}C and Sr was 99.7% and 98.6% respectively. However, the chemical and morphological data suggest that the crystallization pathways involved in precipitation can have a significant impact on the removal of ^{14}C from a solution. If re-crystallization occurs it returns the lattice material to the solution, where it mixes with atmospheric CO_2. This mixing allows dilution of ^{14}C by ^{12}C which results in a lower incorporation of ^{14}C into the re-precipitated calcite. If a treatment system based on calcium hydroxide dosing were applied to the most contaminated groundwater present at the UK Sellafield site, these removals would produce just over 1 kg solid residue (containing ~100 MBq total beta activity) per m^3 treated and produce an effluent with a pH ≤ 9, containing 0.15 KBq L^{-1} of ^{14}C and 0.62 KBq L^{-1} of Sr after a single application.

11. Associated content

This includes additional experimental and XRD data, groundwater compositions, Sr distribution coefficients and reagent costings. Further details of our kinetic model development are also provided along with the full PHREEQC input script. This material is available free of charge via the Internet at http://pubs.acs.org.

Acknowledgements

We thank Andy Connelly, Lesley Neve, Stephen Reid, Fiona Keay and Richard Walshaw (all University of Leeds) for help with BET, XRD, ICP-OES, FIA and SEM analysis respectively. Divyesh Trivedi (National Nuclear Laboratory) is thanked for help during model development. The research was funded by a UK Nuclear Decommissioning Authority PhD bursary to DJH and UK NERC grant NE/L01405X/1 to ITB and DIS.

Appendix A. Supplementary data

Supplementary data to this article can be found online at http://dx.doi.org/10.1016/j.scitotenv.2016.03.192.

References

Achal, V., Pan, X., Zhang, D., 2012. Bioremediation of strontium (Sr) contaminated aquifer quartz sand based on carbonate precipitation induced by Sr resistant Halomonas sp. Chemosphere 89, 764–768. http://dx.doi.org/10.1016/j.chemosphere.2012.06.064.

Amiro, B.D., Ewing, L.L., 1992. Physiological conditions and uptake of inorganic carbon-14 by plant roots. Environ. Exp. Bot. 32, 203–211. http://dx.doi.org/10.1016/0098-8472(92)90003-K.

Aquilonius, K., Hallberg, B., 2005. Process-oriented dose assessment model for 14C due to releases during normal operation of a nuclear power plant. J. Environ. Radioact. 82, 267–283. http://dx.doi.org/10.1016/j.jenvrad.2004.11.009.

Atkins, P., De Paula, J., 2006. Atkins' Physical Chemistry New York WH Freman.

Barton, C.S., Stewart, D.I., Morris, K., Bryant, D.E., 2004. Performance of three resin-based materials for treating uranium-contaminated groundwater within a PRB. J. Hazard. Mater. 116, 191–204. http://dx.doi.org/10.1016/j.jhazmat.2004.08.028.

Bots, P., Benning, L.G., Rickaby, R.E.M., Shaw, S., 2011. The role of SO4 in the switch from calcite to aragonite seas. Geology 39, 331–334.
Boylan, A.A., Stewart, D.I., Graham, J.T., Trivedi, D., Burke, I.T., n.d. Mechanisms of inorganic carbon-14 attenuation in contaminated groundwater: effect of solution pH on isotopic exchange and carbonate precipitation reactions.
Clark, I.D., Fontes, J.-C., Fritz, P., 1992. Stable isotope disequilibria in travertine from high pH waters: laboratory investigations and field observations from Oman. Geochim. Cosmochim. Acta 56, 2041–2050.
Cross, J.E., Ewart, F.T., 1991. HATCHES—a thermodynamic database and management system. Radiochim. Acta 52, 421–422.
Curti, E., 1997. Coprecipitation of Radionuclides: Basic Concepts, Literature Review and First applications. Paul Scherrer Institut.
Dias, C.M., Stenström, K., Bacelar Leão, I.L., Santos, R.V., Nícoli, I.G., Skog, G., Ekström, P., da Silveira Corrêa, R., 2009. $14CO_2$ dispersion around two PWR nuclear power plants in Brazil. J. Environ. Radioact. 100, 574–580. http://dx.doi.org/10.1016/j.jenvrad.2009.03.022.
Fernández-Díaz, L., Fernández-González, Á., Prieto, M., 2010. The role of sulfate groups in controlling $CaCO_3$ polymorphism. Geochim. Cosmochim. Acta 74, 6064–6076.
Fujita, Y., Ferris, F.G., Lawson, R.D., Colwell, F.S., Smith, R.W., 2000. Calcium carbonate precipitation by ureolytic subsurface bacteria. Geomicrobiol J. 17, 305–318.
Gebauer, D., Völkel, A., Cölfen, H., 2008. Stable prenucleation calcium carbonate clusters. Science 322, 1819–1822 (80-.).
Graham, J., 2013. ERT trial groundwater analysis – rounds 16–19. NNL Technical Memorandum LP06489/06/10/07.
Gray, J., Jones, S.R., Smith, A.D., 1995. Discharges to the environment from the Sellafield site, 1951–1992. J. Radiol. Prot. 15, 99–131.
Hall, O.J., Aller, R.C., 1992. Rapid, small-volume, flow injection analysis for ΣCO_2 and NH^{4+} in marine and fresh waters. Limnol. Oceanogr. 37, 1113–1119.
Holland, H.D., Holland, H.J., Munoz, J.L., 1964. The coprecipitation of cations with CaCO3—II. the coprecipitation of Sr^{+2} with calcite between 90° and 100 °C. Geochim. Cosmochim. Acta 28, 1287–1301.
Inskeep, W.P., Bloom, P.R., 1985. An evaluation of rate equations for calcite precipitation kinetics at pCO2 less than 0.01 atm and pH greater than 8. Geochim. Cosmochim. Acta 49, 2165–2180.
Johannsen, K., Rademacher, S., 1999. Modelling the kinetics of calcium hydroxide dissolution in Water. Acta Hydrochim. Hydrobiol. 27, 72–78.
Jung, W.M., Kang, S.H., Kim, W.-S., Choi, C.K., 2000. Particle morphology of calcium carbonate precipitated by gas–liquid reaction in a Couette–Taylor reactor. Chem. Eng. Sci. 55, 733–747.
Katz, A., Sass, E., Starinsky, A., Holland, H.D., 1972. Strontium behavior in the aragonite-calcite transformation: an experimental study at 40–98 °C. Geochim. Cosmochim. Acta 36, 481–496.
Kersting, A.B., Efurd, D.W., Finnegan, D.L., Rokop, D.J., Smith, D.K., Thompson, J.L., 1999. Migration of plutonium in ground water at the Nevada test site. Nature 397, 56–59.
Laker, A., Ashton, C., Cummings, R., 2010. Waste Acceptance Criteria - Low Level Waste Disposal.
Lide, D.R., 2001. CRC Handbook of Physics and Chemistry. CRC.
Magnusson, Å., Stenström, K., Adliene, D., Adlys, G., Dias, C., Rääf, C., Skog, G., Zakaria, M., Mattsson, S., 2007. Carbon-14 levels in the vicinity of the Lithuanian nuclear power plant Ignalina. Nucl. Instrum. Methods Phys. Res., Sect. B 259, 530–535. http://dx.doi.org/10.1016/j.nimb.2007.01.197.
Marinin, D.V., Brown, G.N., 2000. Studies of sorbent/ion-exchange materials for the removal of radioactive strontium from liquid radioactive waste and high hardness groundwaters. Waste Manag. 20, 545–553.
Mayes, W.M., Batty, L.C., Younger, P.L., Jarvis, A.P., Kõiv, M., Vohla, C., Mander, U., 2009. Wetland treatment at extremes of pH: a review. Sci. Total Environ. 407, 3944–3957. http://dx.doi.org/10.1016/j.scitotenv.2008.06.045.
Mitchell, A.C., Ferris, F.G., 2005. The coprecipitation of Sr into calcite precipitates induced by bacterial ureolysis in artificial groundwater: temperature and kinetic dependence. Geochim. Cosmochim. Acta 69, 4199–4210.
Naftz, D., Morrison, S.J., Fuller, C.C., Davis, J.A., 2002. Handbook of Groundwater Remediation Using Permeable Reactive Barriers: Applications to Radionuclides, Trace Metals, and Nutrients. Academic Press.
Nancollas, G.H., Reddy, M.M., 1971. The crystallization of calcium carbonate. II. Calcite growth mechanism. J. Colloid Interface Sci. 37, 824–830.
National Lime Association [WWW Document], n.d. URL https://lime.org/lime-basics/uses-of-lime/construction/building-construction/
National Nuclear Laoratory [WWW Document], n.d. URL http://www.nnl.co.uk/inventory-management/case-studies-and-materials/using-chemical-and-process-modelling-to-design-understand-and-improve-an-effluent-treatment-plant/
NDA, 2013. 5 year Research and Development Plan.
Nielsen, S., 2004. The Biological Role of Strontium Bone.
Nielsen, M.H., Aloni, S., De Yoreo, J.J., 2014. In situ TEM imaging of CaCO3 nucleation reveals coexistence of direct and indirect pathways. Science 345, 1158–1162 (80-.).
Noyes, R.M., Rubin, M.B., Bowers, P.G., 1996. Transport of carbon dioxide between the gas phase and water under well-stirred conditions: rate constants and mass accommodation coefficients. J. Phys. Chem. 100, 4167–4172.
Ostwald, W., 1897. Studien über die Bildung und Umwandlung fester Körper. 1. Abhandlung: Übersättigung und Überkaltung. Z. Phys. Chem. 22, 289–330.
Palmisano, A., Hazen, T., 2003. Bioremediation of Metals and Radionuclides: What it is and How it Works.
Parkhurst, D.L., Appelo, C.A.J., 1999. User's guide to PHREEQC (Version 2): A Computer Program for sPeciation, Batch-reaction, One-dimensional Transport, and Inverse Geochemical Calculations.
Parkhurst, D.L., Appelo, C.A.J., 2013. Description of Input and Examples for PHREEQC Version 3: A Computer Program for Speciation, Batch-reaction, One-dimensional Transport, and Inverse Geochemical Calculations.
Parkman, R.H., Charnock, J.M., Livens, F.R., Vaughan, D.J., 1998. A study of the interaction of strontium ions in aqueous solution with the surfaces of calcite and kaolinite. Geochim. Cosmochim. Acta 62, 1481–1492.
Pingitore Jr., N.E., Lytle, F.W., Davies, B.M., Eastman, M.P., Eller, P.G., Larson, E.M., 1992. Mode of incorporation of Sr^{2+} in calcite: Determination by X-ray absorption spectroscopy. Geochim. Cosmochim. Acta 56, 1531–1538.
Pinsent, B.R.W., Pearson, L., Roughton, Fjw, 1956. The kinetics of combination of carbon dioxide with hydroxide ions. Trans. Faraday Soc. 52, 1512–1520.
Rietveld, H., 1969. A profile refinement method for nuclear and magnetic structures. J. Appl. Crystallogr. 2, 65–71.
Roehl, K.E., Meggyes, T., Simon, F.G., Stewart, D.I., 2005. Long-term Performance of Permeable Reactive Barriers. Gulf Professional Publishing.
Roussel-Debet, S., Gontier, G., Siclet, F., Fournier, M., 2006. Distribution of carbon 14 in the terrestrial environment close to French nuclear power plants. J. Environ. Radioact. 87, 246–259. http://dx.doi.org/10.1016/j.jenvrad.2005.12.002.
Sander, R., 2015. Compilation of Henry's law constants (version 4.0) for water as solvent. Atmos. Chem. Phys.
Saunders, J.A., Toran, L.E., 1995. Modeling of radionuclide and heavy metal sorption around low- and high-pH waste disposal sites at Oak Ridge, Tennessee. Appl. Geochem. 10, 673–684. http://dx.doi.org/10.1016/0883-2927(95)00036-4.
Stamper, A., Coughlin, D., Bowes, A., Ruddick, P., Laws, F., 2014. Groundwater Monitoring at Sellafield Annual Data Review. p. 2013.
Standring, W.J.F., Oughton, D.H., Salbu, B., 2002. Potential remobilization of 137 Cs, 60 Co, 99 Tc, and 90 Sr from contaminated Mayak sediments in river and estuary environments. Environ. Sci. Technol. 36, 2330–2337. http://dx.doi.org/10.1021/es0103187.
Stewart, D., Csõvári, M., Barton, C., Morris, K., 2006. Performance of a Functionalised Polymer-coated Silica at treating uranium contaminated groundwater from a Hungarian Mine site. Eng. Geol. 85, 174–183.
Thompson, A., Steefel, C., 2010. Contaminant desorption during long-term leaching of hydroxide-weathered Hanford sediments. Sci. Technol. 44, 1992–1997.
Tierney, K.M., Muir, G.K.P., Cook, G.T., MacKinnon, G., Howe, J.A., Heymans, J.J., Xu, S., 2016. Accumulation of Sellafield-derived radiocarbon ((14)C) in Irish Sea and West of Scotland intertidal shells and sediments. J. Environ. Radioact. 151 (Pt 1), 321–327. http://dx.doi.org/10.1016/j.jenvrad.2015.10.029.
Zhang, Y., Dawe, R.A., 2000. Influence of Mg^{2+} on the kinetics of calcite precipitation and calcite crystal morphology. Chem. Geol. 163, 129–138.